Ratiometric red aggregation-induced emission luminogens for hydrazine hydrate detection

Xiaofeng Shan [a], Shouting Wu [b], Lingyi Shen [b*], Senlin Peng [b], Hong Xu [a,b*], Zhi-Yong Wang [a,b], Xian-Jiong Yang [a,b], Ya-Li Huang [a,b], Xing Feng[c], Carl Redshaw [d], Qi-Long Zhang [a,b*]

[a] *School of Public Health, the key Laboratory of Environmental Pollution Monitoring and Disease Control, Ministry of Education, Guizhou Medical University, Guiyang 550025, China.*

[b] *School of Basic Medicine, Guizhou Medical University, Guiyang 550025, PR China.*

[c] *Guangdong Provincial Key Laboratory of Functional Soft Condensed Matter, School of Material and Energy, Guangdong University of Technology, Guangzhou 510006, PR China.*

[d] *Chemistry, School of Natural Sciences, University of Hull, Cottingham Road, Hull, Yorkshire HU6 7RX, UK.*

*Corresponding author. Tel.: 086 851 88174018; Fax: 086 851 88174018.

E-mail addresses: shenly@stumail.nwu.edu.cn (Lingyi Shen); xuhong@gmc.edu.cn (H. Xu); gzuqlzhang@126.com (Q. L Zhang).

Abstract: Based on a deprotection reaction and intramolecular charge transfer (ICT) mechanism induced by hydrazine hydrate, a fluorescent probe for the rapid recognition of hydrazine hydrate ($N_2H_4 \cdot H_2O$) was designed. A simple one-step condensation reaction was employed to synthesize a series of novel aggregation-induced emission fluorescent probes with good sensitivity and selectivity for $N_2H_4 \cdot H_2O$. The detection limits for $N_2H_4 \cdot H_2O$ using **1** to **3** were 1.51, 0.544 and 2.61 μM, respectively, at a probe concentration of 20.0 μM. Furthermore, probes **1-3** were able to detect $N_2H_4 \cdot H_2O$ in living cells and it was found that probes **1-3** could interact with $N_2H_4 \cdot H_2O$ to provide

an effective tool for on-line monitoring. Moreover, probe **1** is capable of the imaging and tracing of $N_2H_4 \cdot H_2O$ in zebrafish.

KEYWORDS: Aggregation-induced emission; Deprotection reaction; Intramolecular charge transfer mechanism; Hydrazine hydrate; Zebrafish

1. Introduction

Hydrazine hydrate ($N_2H_4 \cdot H_2O$) is an inorganic dual amine, and a colorless liquid with an ammonia-like odor. Given its nucleophilicity and strong alkalinity, hydrazine hydrate and its derivatives play an important role in the fields of pharmaceuticals, agrochemicals and fine chemicals [1]. In industrial production, hydrazine hydrate is widely used in the synthesis of catalysts [2-6], agricultural chemicals [7-11], pharmaceuticals (synthesis of anti-diabetic drugs, anti-tuberculosis drugs) [12-16] and foaming agents [17]. For the mass production methods often employed in industry, even a small amount of hydrazine hydrate leaking can cause irreversible damage to the environment. Moreover, there is the risk that human beings will come into contact with residual hydrazine hydrate, and this poses a threat to human health given the associated toxicity and potential carcinogenic effects. It can be absorbed through the respiratory tract or skin, and a series of symptoms such as mild dizziness and central nervous system excitement may occur in the short term. Long-term exposure to hydrazine hydrate may cause serious damage to human viscera such as liver, lung, kidney and the nervous system [18-19]. According to the USEPA (U.S. Environmental Protection Agency) [20-23], the amount of hydrazine hydrate residue in drinking water should be

less than 10 ppm. Prolonged exposure to high levels of hydrazine can cause irreparable damage to the central nervous system. In addition, some drugs in the physiological metabolism of the human body, such as isoniazid ($C_6H_7N_3O$) [24-26], will also release hydrazine molecules, which can cause serious harm. Therefore, it is important to design and develop a qualitative and quantitative detection method for hydrazine hydrate.

In recent years, the analytical methods reported in the literature for hydrazine hydrate detection mainly include HPLC (High Performance Liquid Chromatography) [27], electrochemical methods [28], titration methods [29] and spectrophotometry [30]. However, these methods are not suitable for field analysis because they require cumbersome samples and reagent preparation processes or complex instrumentation. The fluorescence analysis method has the advantages of good selectivity, high sensitivity and strong real-time imaging ability [31-33]. Continuous research efforts have led to the development of hydrazine hydrate small molecule fluorescent probes. To date, fluorescent probes have developed rapidly in the field of detection and are widely used in the detection of small molecules, biomolecules and intracellular ions [34-37]. However, there are relatively few fluorescent probes for the quantitative detection of hydrazine hydrate [38-40]. Therefore, it is of great significance to develop an effective fluorescent probe with ideal sensitivity, response speed and biocompatibility for the quantitative detection of hydrazine hydrate. At present, reports on hydrazine hydrate probes are mainly based on the following reaction mechanisms: hydrazine hydrate deprotects the leulinic acid group, the substitution reaction of hydrazine hydrate to malononitrile group, hydrazine hydrate deprotects phthalimide,

and hydrazine hydrate deprotects butyryl ester at the 4-position. These methods greatly facilitate the development of hydrazine fluorescent probes [41-46]. The design of substitution reactions of hydrazine hydrate at the malonitrile group has received much attention because of the simplicity of synthesis and selection specificity.

A number of fluorescent probes have been reported that detect hydrazine although some still have drawbacks. These include the traditional aggregation phenomenon which leads to probe quenching (ACQ), the fluorescence probe emission wavelength and small Stokes displacement, which will cause the fluorescence probe quenching and fluorescence detection error [47,48]. This means that the shortcomings may limit their further use. Therefore, designing a multifunctional hydrazine fluorescent probe with long emission wavelength and a large Stokes shift is necessary.

Herein, we have developed a series of red fluorescent probes **1**-**3** (Scheme 1) for the recognition of hydrazine by a simple one-step condensation reaction. The resulting probes exhibit remarkable aggregation-induced emission and a large Stokes shift on increasing the proportion of water present. Moreover,, their ability to trace $N_2H_4 \cdot H_2O$ in living cells and zebrafish has been investigated. DFT calculations, UV-vis absorption spectra and fluorescence spectra revealed conversion to the corresponding hydrazone which inhibits the intramolecular charge transfer (ICT) process.. Experimental results proved that the probes **1**-**3** have good selectivity and high sensitivity for the detection of hydrazine, whilst probe **1** is capable of the quantitative detection of hydrazine in cell systems and zebrafish. In addition, probes **1**-**3** also demonstrated good optical properties thereby providing a potential molecular tool for real-time tracking.

2. Experimental

2.1 Chemicals and reagents

Unless otherwise stated, all chemicals and solvents (Et_2O, THF, Toluene, Hexane, EtOH, $CHCl_3$ and CH_2Cl_2) used were purchased from commercial sources and were used without further purification. and the experimental water was ultrapure water.

2.2 Characterization

Bruker AVANCE NEO 600M NMR (Bruker AXS Company, Germany); Xevo G2-S QT of MS spectrometer (Waters, USA); Cary Eclipse type fluorescence spectrophotometer (Varian Company, USA); pH meter of pHS-25 (Chengdu Century Ark Technology Co., Ltd., China); UV-VIS spectrophotometer of UV-2700 (SHIMADZU (HONG KONG) LIMITED China); BRUKER D8 Venture (Bruker AXS Company, Germany). Laser scanning confocal microscope FV-1000 (Olympus Corporation, Japan); Forma 3111 Water jacket CO_2 incubator (Forma Corporation, USA); Zebrafish breeding equipment (Beijing Aisheng Technology Co, LTD.); Decolorizing shaker (Jintan Zhengji Instrument Factory HY-4, Jiangsu, China). FLS1000 Photoluminescence Spectrometer (Edinburgh Instruments Ltd, England); Nicolet Magna 750FT-IR spectrometer.

2.3 Synthesis of the fluorescent probes **1-3**

0.36 g (1.0 mmol) 5-(4-(diphenylamino)phenyl) thiophene-2-carbaldehyde and 0.13 g (2.0 mmol) malononitrile were mixed in 20 mL anhydrous ethanol and stirred at 85 ℃ for 2 h, and then the solution was cooled to room temperature. Then, the solvent

was removed under reduced pressure, and the crude product was repeatedly washed with ethanol and dried to obtain a reddish-brown powder **1** (0.19 g) with a yield of 40%. m.p: 125~126℃. ^{1}H NMR (600 MHz, DMSO-d_6) δ 8.60 (s, 1H, vinyl-H), 7.92 (d, J = 4.1 Hz, 1H, thiophene-H), 7.70 (m, 3H, thiophene-H, Ar-H), 7.37 (t, J = 7.8 Hz, 4H, Ar-H), 7.16 (t, J = 7.4 Hz, 2H, Ar-H), 7.12 (d, J = 8.0 Hz, 4H, Ar-H), 6.96 (d, J = 8.7 Hz, 2H, Ar-H). ^{13}C NMR (150 MHz, d_6-DMSO) δ (ppm): 155.5, 152.3, 149.1, 146.1, 142.7, 132.9, 129.7, 127.7, 125.2, 124.4, 124.2, 121.1, 114.8, 114.0, 73.2. MS (HR-ESI): calcd for $C_{26}H_{17}N_3S$ [M^+]: 403.1138; found: 403.1132. IR (KBr pellet, cm^{-1}): 3020 (w), 2220 (m), 1560 (vs), 1490 (s), 1420 (vs), 1320 (s), 1280 (m), 1070 (m), 801 (w), 756 (m), 701 (w), 600 (w), 515 (w) (Figs. S1–S4).

Probe **2** was synthesized by a similar synthetic procedure to probe **1** affording a reddish-brown solid in 46% yield. m.p: 161~162℃. ^{1}H NMR (600 MHz, DMSO-d_6) δ (ppm): 8.57 (s, 1H, vinyl-H), 7.90 (d, J = 4.2 Hz, 1H,), 7.65 (dt, J = 9.5, 2.4 Hz, 3H, thiophene-H, Ar-H), 7.17 (d, J = 8.2 Hz, 4H, Ar-H), 7.01 (d, J = 8.3 Hz, 4H, Ar-H), 6.89-6.85 (m, 2H, Ar-H), 2.29 (s, 6H, CH_3-H). ^{13}C NMR (150 MHz, DMSO-d_6): δ (ppm): 155.8, 152.2, 149.5, 143.5, 142.7, 133.8, 132.6, 130.2, 127.6, 125.5, 123.5, 119.7, 114.8, 114.0, 72.8, 20.4. MS (HR-ESI): calcd for is $C_{28}H_{21}N_3S$ [M^+]: 431.1451; found: 431.1447. IR (KBr pellet, cm^{-1}): 3030 (w), 2210 (s), 1600 (m), 1570(vs), 1510 (s), 1430 (vs), 1360 (s), 1320 (s), 1290 (s), 1190 (m), 1070 (m), 939 (w), 814 (s), 724 (w), 592(w), 512 (w) (Figs. S5–S8).

Probe **3** was synthesized by a similar procedure to **1**, affording a reddish-brown solid in 51% yield. m.p: 152~153 ℃. ^{1}H NMR (600 MHz, DMSO-d_6) δ (ppm): 8.52 (s,

1H, vinyl-H), 8.02 (dd, J = 9.7, 3.1 Hz, 2H, Ar-H), 7.94–7.88 (m, 2H, Ar-H), 7.73 (t, J = 6.0 Hz, 2H, Ar-H), 7.36 (dd, J = 10.9, 4.8 Hz, 4H, Ar-H), 7.11 (dd, J = 17.3, 7.5 Hz, 6H, Ar-H), 7.02 (t, J = 5.4 Hz, 2H, Ar-H). ^{13}C NMR (150 MHz, DMSO-d_6): δ (ppm): 161.5, 148.1, 146.5, 145.1, 131.2, 131.0, 129.5, 128.0, 126.5, 124.7, 123.8, 122.0, 114.4, 113.5, 70.7. MS (HR-ESI): calcd for is $C_{28}H_{19}N_3$ [M^+]: 397.15735; found: 397.15736. IR (KBr pellet, cm^{-1}): 3030 (w), 2220 (m), 1580 (vs), 1540 (m), 1490 (vs), 1420 (w), 1330 (s), 1270 (vs), 1200 (s), 1170 (m), 939 (w), 824 (m), 754 (m), 692 (m), 612 (w), 512 (m). (Figs. S9–S12).

Probe **1**-NH_2NH_2 is a yellow solid. m.p: 217~218 ℃. ^{1}H NMR (600 MHz, DMSO-d_6) δ 7.84 (s, 1H, vinyl-H), 7.53 (d, J = 8.4 Hz, 2H, Ar-H), 7.32 (m, 4H, Ar-H), 7.27 (d, J = 3.6 Hz, 1H, thiophene-H), 7.07 (m, 2H, Ar-H), 7.04 (d, J = 7.8 Hz, 4H, Ar-H), 7.00 (d, J = 3.6 Hz, 1H, thiophene-H), 6.96 (d, J = 8.4 Hz, 2H, Ar-H); 6.80 (s, 2H, amino-H). MS (HR-ESI): calcd for is $C_{23}H_{20}N_3S$ [M+H]$^+$: 370.1372; found: 370.1378. IR (KBr pellet, cm^{-1}): 3060 (w), 2036 (m), 1590 (vs), 1490 (vs), 1440 (vs), 1320 (m), 1280 (s), 1190 (w), 1060 (w), 1020 (w), 834 (w), 799 (m), 754 (m), 694 (s), 617 (w), 512 (w). Solution Quantum Yield (Φ): 5.27%; Solid Quantum Yield (Φ): 0.27%.

2.4 General methods for optical tests

Preparation of probe stock solution and analyte solution: The correct amount of the probe was placed in acetonitrile and prepared as a 1.0 mmol/L stock solution. The metal ions (Na^+, Pb^{2+}, Fe^{3+}, Ni^{2+}, Hg^{2+}, Co^{2+}, Cr^{3+}, Cu^{2+}, Li^+, K^+, Mg^{2+}, Al^{3+}, Zn^{2+}, Ag^+, Cd^{2+}), Anions (CO_3^{2-}, Br^-, HCO_3^-, AcO^-, HSO_3^-, ClO_4^-, Cl^-, CN^-, NO_2^-, NO_3^-, SO_4^{2-},

PO_4^{3-}, F^-, $H_2PO_4^-$, $S_2O_3^{2-}$, HPO_4^{2-}, I^-, SO_3^{2-},$C_2O_4^{2-}$, S^{2-}) and amino-containing small molecules (Cys, GSH, Urea, Hcy, Butylamine ($C_4H_{11}N$), NH_3, DMF, INH, TEA, TEOA) were prepared at a concentration of 10 mM ionogen solution. The concentration of the $N_2H_4 \cdot H_2O$ solution was 0.2 mM. The PBS buffer solution of the specific pH required for the experiment was prepared by adjusting the sodium hydroxide (0.5 M) or hydrochloric acid (0.5 M). All fluorescence spectra and UV-vis absorption measurements of the test solution (probe stock (100 μL) and each specific solution in 5 mL sample tubes) were performed at room temperature unless otherwise noted.

3. Results and discussion

3.1 Synthesis

To construct the donor–π–acceptor (D–π–A) type probes, triphenylamine was selected as the electron donor, malononitrile as the electron acceptor and as the recognition group hydrazine hydrate. Therefore, the probe **1** was formed via the commercially available precursor 5-(4-(diphenylamino)phenyl)thiophene-2-carbaldehyde with malononitrile under 85 °C for 2 h in anhydrous ethanol (Scheme 1). 5-(4-(Di-p-tolylamino)phenyl)thiophene-2-carbaldehyde and 4'-(diphenylamino)-[1,1'-biphenyl]-4-carbaldehyde were then used to condense with malononitrile, respectively, affording probes **2** and **3**. The structures of these probes were characterized using ^1H and ^{13}C NMR spectroscopy and high-resolution mass spectrometry (HRMS). Moreover, X-ray crystallography further confirmed their structures as shown in Fig. 1 and the crystallographic data are given in Table S1; CCDC numbers: Probe **1**, 2261613; Probe **2**, 2261614; Probe **3**, 2261615.

3.2 AIE properties of the probes **1-3**

To gain a detailed understanding of the Aggregation-Induced Emission (AIE) behavior of the probes **1-3** in solution, the fluorescence spectra of the probes **1-3** were first evaluated in different solvents. As shown in Figs. 2A and S10, the fluorescence emission from probes **1-3** in most common organic solvents ranged from 583 to 670 nm, 584 to 718 nm and 579 to 673 nm, respectively (Fig. S13). The results showed that probes **1-3** exhibited good solubility in these solvents, while being only slightly affected by the solvent polarity. The AIE properties of the probes **1-3** was studied in acetonitrile/water mixtures with different water fractions (f_w), which allowed for a certain extent of solute aggregation. In acetonitrile solution, probes **1-3** weakly emit red fluorescence, with quantum yields of 0.04-2.14% (Table S3). All three compounds show a gradual increase in fluorescence intensity on raising the fraction of water from 70%. The strongest fluorescence intensities were found with a 95% fraction of water upon aggregation, in which their fluorescence intensities were enhanced to about 586-, 363-, and 428-fold compared to those in acetonitrile solution (Fig. 2B). Their quantum yields (7.86, 7.68 and 9.13%) in the solid state also dramatically increased compared with those in solution (Table S3). Their maximum emissions in the aggregation state are located at 664, 680, and 625 nm, indicative of their NIR-emissive properties (Fig. 2A). In addition, redshifts of emissions are observed from the aggregate to the solid state, for which the fluorescence spectra peaked at 695, 712, and 632 nm (Fig. S14). The data indicate that probes **1-3** have classic AIE properties. In addition, these fluorescent probes have significant Stokes shifts of 181, 188, and 184 nm, respectively.

3.3 Detecting $N_2H_4 \cdot H_2O$

In complex biological samples, highly selective responses are required to perceive the properties necessary for the target species. To verify the probe compounds specific recognition of $N_2H_4 \cdot H_2O$, and that they can achieve the detection of $N_2H_4 \cdot H_2O$ under biologically relevant conditions, the presence of some common ions and molecules (Na^+, Pb^{2+}, Fe^{3+}, Ni^{2+}, Hg^{2+}, Co^{2+}, Cr^{3+}, Cu^{2+}, Li^+, K^+, Mg^{2+}, Al^{3+}, Zn^{2+}, Ag^+, Cd^{2+}, CO_3^{2-}, Br^-, HCO_3^-, AcO^-, HSO_3^-, ClO_4^-, Cl^-, CN^-, NO_2^-, SO_4^{2-} PO_4^{3-}, F^-, $H_2PO_4^-$, $S_2O_3^{2-}$, HPO_4^{2-}, I^-, SO_3^{2-}, $C_2O_4^{2-}$, S^{2-}, Hcy, Cys, Urea, GSH, Butylamine ($C_4H_{11}N$), NH_3, DMF, INH, TEA, TEOA) was investigated. As shown in Figs. 3 and S15-S17, $N_2H_4 \cdot H_2O$ stimulated significant fluorescence enhancement of the probes **1-3**, while the presence of the other ions and molecules had little effect on the fluorescence of the probes. In addition, anti-interference experiments were carried out. Spectral data show that the addition of coexisting substances in the reaction system between probes **1-3** and $N_2H_4 \cdot H_2O$ does not significantly interfere with the detection ability of the probe (Figs. 4 and S18-S19).

Furthermore, we investigated the fluorescence response of probe **1** (20 μM, pH= 7.4, acetonitrile / H_2O =1 / 4) toward $N_2H_4 \cdot H_2O$. The results are shown in Fig. 5A, where the blank probe **1** test solution exhibited red fluorescence with a peak emission at 665 nm.

Upon addition of $N_2H_4 \cdot H_2O$, probe **1** revealed a new fluorescence emission at 467 nm. The intensity at 467 nm gradually increases on increasing $N_2H_4 \cdot H_2O$ concentration and gradually decreases at 665 nm. Moreover, probe **1** changes from bright red to blue-

green fluorescence at this time under 365 nm UV light. As the $N_2H_4 \cdot H_2O$ concentration increases to 20 μM, the fluorescence curve no longer rose and reached a plateau. Meanwhile, the change in fluorescence intensity at 467 nm varies linearly with the concentration of N_2H_4 (0–20 μM). As shown in Fig. 5B, the linear equation is $y = 47.96x - 10.989$, and the correlation coefficient is $R^2 = 0.9910$. Based on this linear equation and the underlying formula $3\sigma/k$, (σ is the standard deviation of the fluorescence intensity of the ten times blank probe solution, and *k* is the slope of the linear equation), the lowest detection limit was calculated to be 1.51 μM.

Given the likely complex detection environment, good pH stability is a necessary pre-requisite for the probe. We tested the effect of different pH buffer systems (acetonitrile / H_2O (v / v= 1 / 4, pH= 2.0-12.0) on the probe. As shown in Fig. 5C, probe **1** remained stable at different pH (pH= 2.0-12.0) and readily recognizes $N_2H_4 \cdot H_2O$ in a pH=3-11 buffer system. Thus, this indicates that probe **1** has good stability in different pH environments. After that, we proceeded to investigate the response time of probe **1** toward $N_2H_4 \cdot H_2O$. As shown in Fig. 5D, probe **1** reached a steady state after interacting with saturating concentrations of $N_2H_4 \cdot H_2O$ for about 110 min. The optical properties of probes **2, 3** for sensing $N_2H_4 \cdot H_2O$ are shown in the Supporting Information Figs. S20–S21 and are summarized in Table 1.

3.4 Mechanism for sensing $N_2H_4 \cdot H_2O$

To explore the mechanism of the interaction between the probes and $N_2H_4 \cdot H_2O$, DFT calculations were conducted using the Gaussian 09 program (B3LYP/6-31 G(d)) in order to determine the electronic structure of probe **1** and probe **1**+N_2H_4 adduct. As

shown in Fig. 6, electrons transfer from the electron-donating triphenylamine to the electron-drawing malonitrile from HOMO to LUMO orbitals in probe **1**, indicating a significant ICT. This is the main reason for the weak fluorescence-emission of probe **1**. In contrast in probe **1**+N_2H_4 adduct, the dissociation of π-electrons is weakened, which interferes with the ICT process and results in a significant green fluorescence enhancement. In addition, the energy gap of probe **1** (ΔE= 2.43 eV) is smaller than that of probe **1**+N_2H_4 adduct. (ΔE = 3.33 eV), which leads to the blue-shift emission in the presence of N_2H_4, as demonstrated by the experimental results of the UV-vis and fluorescence spectra. The DFT calculation results for probes **2** and **3** are shown in Fig. S22.

Based on the above results and the literature relating to the recognition mechanism of $N_2H_4·H_2O$ with fluorescent probes [49-52], we suspect that the mononitrile group of probe **1** is not only the absorbing electron group in the typical D-π-A structure, but also the reaction site of $N_2H_4·H_2O$. After interacting with $N_2H_4·H_2O$, the malononitrile has been damaged by the ICT process, which has affected the distribution of electron density in the molecule, resulting in the identification of the changes in the absorption spectra and fluorescence spectra. The reaction process of probe **1** for the recognition of $N_2H_4·H_2O$ is proposed as shown in Scheme 2.

Probe **1** reacts with $N_2H_4·H_2O$ to form hydrazine, using the malononitrile group as the recognition group, which changes the push-pull structure and results in changes in the spectrum. On gradual addition of $N_2H_4·H_2O$, the fluorescence spectrum of the probe changes, new emission peaks appear, and the fluorescence changes from bright

red to blue-green. At the same time, the maximum absorption peak of the probe gradually decreased, whilst the new absorption peak and the solution color gradually faded. Fortunately, the probe **1**-NH_2NH_2 adduct was isolated and characterized (Figs. S23-S25). The ^1H NMR and HRMS spectra fully verified the predicted structure of the probe **1**-NH_2NH_2 adduct. Moreover, the disappearance of the peak for the C≡N group (ν= 2220 cm^{-1}) accompanying by the appearance of a peak for the –NH_2 group (ν= 3060 cm^{-1}) in the IR spectrum gives further insight into the adduct. Meanwhile, the solution quantum yield (5.27%) and solid quantum yield (0.27%) also exhibits a expectedly change when compared with probe **1** (Table S3).

3.5 Detection applications in living cells

To extend the detection of probe $N_2H_4 \cdot H_2O$ in living cells, we first examined the cytotoxicity of probes **1-3** (Fig. S26). The results showed more than 80% survival of HeLa cells incubated for 24h over the range 0-25 μM. This indicates that probes **1**–**3** have low cytotoxicity over a relatively low concentration range and are suitable for bioimaging experiments. Therefore, they would be biosafe when applied to cell imaging experiments at a sensor concentration of 10 μM.

In order to further verify the ability of probes **1-3** to detect actual samples, HeLa cells were selected as cell imaging carriers in the experiment to evaluate the biological ability of the probes to monitor $N_2H_4 \cdot H_2O$ in living cells (as shown in Figs. 7 and S27-S28). We incubated the cells with a 10 μM probe for 30 min and observed them under a laser confocal microscope. The results showed that the incubated cells showed a bright red in the red channel. Subsequently, the cells were further treated with 10 μM

hydrazine for 1h, and we observed diminished red fluorescence in the cells and a concurrent green fluorescence (green channel). Furthermore, the respective fluorescence intensities of probes **1-3** in the cells visually show the fluorescence changes in the presence of $N_2H_4 \cdot H_2O$.

3.6 Fluorescence imaging in zebrafish

Based on the above cell imaging results, we further investigated the possibility of probe **1** for detecting $N_2H_4 \cdot H_2O$ *in vivo*. We chose the zebrafish as a model animal. The results are illustrated in Fig. 8, and as for the cellular phenomena, probe **1** showed red fluorescence in zebrafish, whereas probe **1** (5 μM) showed green fluorescence in zebrafish after treatment with $N_2H_4 \cdot H_2O$ (5 μM). Therefore, these results indicate that probe **1** has the ability to trace $N_2H_4 \cdot H_2O$ in living biological systems.

4. Conclusions

In summary, based on the ICT mechanism, we have prepared via a one-step reaction three AIE near infrared fluorescent probes **1-3** which exhibit good selectivity and high sensitivity for the detection of $N_2H_4 \cdot H_2O$. Upon interaction with $N_2H_4 \cdot H_2O$, the probe undergo a nucleophilic reaction which removes the protective group, enhancing the ICT effect and resulting in enhanced fluorescence intensity. Probes **1-3** have low detection limits, which allows the probes the potential to detect $N_2H_4 \cdot H_2O$ both qualitatively and quantitatively in real samples. Furthermore, the successful detection of $N_2H_4 \cdot H_2O$ in live cells and in zebrafish suggests that probe **1** is available for the detection of biological systems. We expect probes **1-3** will be a versatile useful tool for the detection of $N_2H_4 \cdot H_2O$ in multiple fields, and believe this work provides a

new example of a small molecular probe for ion detection.

Acknowledgements

This work was supported by and the National Natural Science Foundation of China (22066007, 22065009), the Guizhou Provincial Natural Science Foundation (grant number ZK[2022]395, grant number [2018] 5779-14). Guizhou Medical University Startup Project of Doctor Scientific Research (grant number YJ2020-BK024), Cultivation program of the Guizhou Medical University (20NSP012), CR thanks the University of Hull for support.

Supplementary data

Electronic Supplementary Information (ESI) available: Details of the NMR and MS spectrum, AIE properties of the probe, Cell Cytotoxicity and the Probe viscosity correlation.

References

[1] Liu B, Liu Q, Shah M, Wang J, Zhang G, Pang Y. Fluorescence monitor of hydrazine in vivo by selective deprotection of flavonoid. SENSORS AND ACTUATORS B. 202 (2014) 194-200.

[2] Song F, Liang R, Deng J, Liu Z, Peng X. Fine-tailoring the linker of near-infrared fluorescence probes for nitroreductase imaging in hypoxic tumor cells. Chinese Chemical Letters. 2017; 28 (10): 4.

[3] Jiang C, Yao Y, Kong C, Du J, Meng J, Yao C. A novel colorimetric and ratiometric fluorescent probe for targeted detection of hypochlorous acid based on HClO-mediated anthracene-

hydrazone to anthracene-triazole transformation. Analytical Methods. 2019;11.

[4] Pan X, Zhong Y, Jiang Y, Zuo G, Li J, Dong W. Reaction-based fluorescent sensor for detection of bisulfite through 1,4-addition reaction in water. Materials Chemistry and Physics. 2018;213:83-8.

[5] A MM, A MB, A AS, A TS, A ST, B AG, et al. Optical sensors for detection of nano-molar Zn^{2+} in aqueous medium: Direct evidence of probe- Zn2+ binding by single crystal X-ray structures - ScienceDirect. Journal of Photochemistry and Photobiology A: Chemistry. 2019; 368: 52-61.

[6] Wu C, Xu H, Li Y, Xie R, Li P, Pang X, et al. A "naked-eye" colorimetric and ratiometric fluorescence probe for trace hydrazine. Analytical Methods. 11 (2019) 2591-2596.

[7] Yang Y, He L, Xu K, Lin W. Development of a mitochondria-targeted fluorescent probe for the ratiometric visualization of sulfur dioxide in living cells and zebrafish. Analytical Methods. 2019; 11(31): 3931-5.

[8] Zhang Y, Wang B, Yue X, Han J, Song X, Wang J. A ratiometric merocyanine-based fluorescent probe for detecting hydrazine in living cells and zebra fish. Chinese Chemical Letters. 2020; 31 (06): 1508-10.

[9] Taleb, Abdinejad, Mohammad, R., Zamanloo, Nosrat, et al. Colorimetric sensing of cyanide ion by pyromellitic diimides synthesized in one step from commercially available reactants. Journal of Photochemistry & Photobiology A Chemistry. 371 (2019) 17-24.

[10] M.M. Xing, K.N. Wang, X.W. Wu, S.Y. Ma. A coumarin chalcone ratiometric fluorescent probe for hydrazine based on deprotection, addition and subsequent cyclization mechanism. Chemical Communications. 55 (2019) 14980-14983.

[11] Jung, Park, Kang, Kim. Hydrazine-Selective Fluorescent Turn-On Probe Based on Ortho-

Methoxy-Methyl-Ether (o-MOM) Assisted Retro-aza-Henry Type Reaction. Sensors. 2019; 19 (20): 4525.

[12] Mehta PK, Oh ET, Park HJ, Lee KH. Ratiometric fluorescent probe based on symmetric peptidyl receptor with picomolar affinity for Zn2+ in aqueous solution. Sensors and Actuators B Chemical. 2017; 245 (jun.):996-1003.

[13] C.Y. Wu, H. Xu, Y.Q. Li, R.H. Xie. An ESIPT-based fluorescent probe for the detection of phosgene in the solution and gas phases. Talanta. 200 (2019) 78-83.

[14] Meng X, DuanlinHu, ZhiyongHan, XinghuaLi, ZhichunLiang, DongMa, Wenbing. A coumarin based highly selective fluorescent chemosensor for sequential recognition of Cu2+ and PPi. Tetrahedron letters: The International Journal for the Rapid Publication of Preliminary Communications in Organic Chemistry. 2018; 59 (49).

[15] Wu Q, Zheng J, Zhang W, Wang J, Liang W, Stadler FJ. A new quinoline-derived highly-sensitive fluorescent probe for the detection, of hydrazine with excellent large-emission-shift ratiometric response. Talanta: The International Journal of Pure and Applied Analytical Chemistry. 2019 (195-):195.

[16] Lan J, Guo J, Jiang X, Chen Y, Hu Z, Que Y, et al. A new dicyanoisophorone-based ratiometric and colorimetric near-infrared fluorescent probe for specifically detecting hypochlorite and its bioimaging on a model of acute inflammation. Analytica Chimica Acta. 2020; 1094: 70-9.

[17] Li J, YingGuo, HaoranLi, XiaokangTang, HaoyangLi, JianGuo, Yuan. A novel colorimetric and ratiometric fluorescent probe for selective detection of bisulfite in real samples and living cells. Dyes and Pigments. 2019; 163.

[18] Ding Y, Zhao S, Wang Q, Yu X, Zhang W. Construction of a coumarin based fluorescent

sensing platform for palladium and hydrazine detection. Sensors and Actuators. 2018; B256 (MAR.): 1107-13.

[19] Chen Z, Zhong X, Qu W, Shi T, Wang S. A highly selective HBT-based "turn-on" fluorescent probe for hydrazine detection and its application. Tetrahedron Letters. 2017; 58 (26).

[20] Zhang WJ, Liu SG, Han L, Luo HQ, Li NB. A ratiometric fluorescent and colorimetric dual-signal sensing platform based on N-doped carbon dots for selective and sensitive detection of copper(II) and pyrophosphate ion. Sensors & Actuators B: Chemical. 2019; 283.

[21] Yang X, Yang Y, Zhou T, Jin M, Jing X, Miao CH, et al. A mitochondria-targeted ratiometric fluorescent probe for detection of SO2 derivatives in living cells and *in vivo*. Journal of Photochemistry and Photobiology A: Chemistry. 2018; 372: 212-7.

[22] Xu M, Huang W, Lu D, Huang C, Zhou T. Alizarin Red-Tb3+ complex as ratiometric colorimetric and fluore-scent dual probe for the smartphone-based detection of anthrax biomarker. Analytical Methods. 2019; 11 (33).

[23] Niu T, Yu T, Yin G, Chen H, Yin P, Li H. A novel colorimetric and ratiometric fluorescent probe for sensing SO_2 derivatives and their bio-imaging in living cells. Analyst. 2019;144.

[24] Liu K, ShiyiGuo, PingLiu, LijuanShi, XuefangZhu, Bolin. A novel fluoro-chromogenic Cu2+ probe for living-cell imaging based on rhodamine 6G-pyridine conjugation. Analytical and bioanalytical chemistry. 2019; 411 (14).

[25] Wang Z, LiHao, YuminDong, WenjuanLiu, YangSong, ShengmeiShuang, ShaominDong, ChuanGong, Xiaojuan. Ratiometric fluorescent sensors for sequential on-off-on determination of riboflavin, Ag+ and L-cysteine based on NPCl-doped carbon quantum dots. Analytica chimica acta. 2021; 1144 (1).

[26] Georgiev N, ISaid, Awad, IToshkova, Reneta A.Tzoneva, Rumiana D.Bojinov, Vladimir B. A novel water-soluble perylenetetracarboxylic diimide as a fluorescent pH probe: Chemosensing, biocompatibility and cell imaging. Dyes and Pigments. 2019; 160.

[27] Jiao S, Wang X, Sun Y, Zhang L, Sun W, Sun Y, et al. A novel fluorescein-coumarin-based fluorescent probe for fluoride ions and its applications in imaging of living cells and zebrafish *in vivo*. Sensors & Actuators. 2018; B262 (JUN.): 188-94.

[28] Lin L, Liang X, Xu Y, Yang Y, Dai Z. Doxorubicin and Indocyanine Green Loaded Hybrid Bicelles for Fluorescence Imaging Guided Synergetic Chemo/Photothermal Therapy. Bioconjug. Chem. 2017; 28(9): 2410.

[29] Zhang Q, Li Y, Zuo H, Wang C, Shen Y. A new colorimetric and ratiometric chemodosimeter for mercury (II) based on triphenylamine and benzothiadiazolenovel. Journal of Photochemistry and Photobiology A Chemistry. 2016; 332: 293-8.

[30] Leng T, Ma Y, Chen G. A novel ratiometric fluorescence and colorimetric probe with a large stokes shift for Hg2+ sensing. Journal of Photochemistry and Photobiology A: Chemistry. 2018; 353: 143-9.

[31] Tianyi, Qin, Bin, Liu, Yingying, Huang, et al. Ratiometric fluorescent monitoring of methanol in biodiesel by using an ESIPT-based flavonoid probe. Sensors & Actuators B Chemical. 2018; 277.

[32] Wu K, Zhang T, Wang Z, Wang L, Zhan L, Gong S, et al. De Novo Design of Excited-State Intramolecular Proton Transfer Emitters via a Thermally Activated Delayed Fluorescence Channel. Journal of the American Chemical Society. 2018; 140(28): 8877-86.

[33] Liang X, Zhang L, Xu X, Qiao D, Shen T, Yin Z, et al. An ICT-Based Mitochondria-Targeted

Fluorescent Probe for Hydrogen Peroxide with a Large Turn-On Fluorescence Signal. ChemistrySelect. 2019; 4(4): 1330-6.

[34] P. Hou, Y.J. Dong, S. Li, F. X., Bioimaging of reactive coumarin N_2H_4 fluorescent probe, China Measurement and Test. 2017; 226: 53-7.

[35] S. Chen, J. Wang, P. Hou, L. Liu, X. Wang, Synthesis and application of a novel naphthimide fluorescent probe for the detection of biological mercaptan, China Measurement and Test. 2016; 217: 64-7.

[36] Lee S, Li J, Zhou X, Yin J, Yoon J. Recent progress on the development of glutathione (GSH) selective fluorescent and colorimetric probes. Coordination Chemistry Reviews. 2018; 366: 29-68.

[37] Z.L. Wang, Y. Zhang, J. Song, Y.Q. Yang, X. Xu, M.X. Li, H.J. Xu, S.F. Wang. A novel isolongifolanone based fluorescent pochlorite and its application in bio-imaging. Analytica Chimica Acta. 2019; 1051: 169-178.

[38] Choi MG, Hwang J, Moon JO, Sung J, Chang SK. Hydrazine-Selective Chromogenic and Fluorogenic Probe Based on Levulinated Coumarin. Organic Letters. 2011; 13(19): 5260-3.

[39] Raju MVR, Prakash EC, Chang HC, Lin HC. A facile ratiometric fluorescent chemodosimeter for hydrazine based on Ing–Manske hydrazinolysis and its applications in living cells. Dyes and Pigments. 2014; 103: 9–20.

[40] Zhou J, Shi R, Liu J, Wang R, Xu Y, Qian X. An ESIPT-based fluorescent probe for sensitive detection of hydrazine in aqueous solution. Organic & Biomolecular Chemistry. 2015; 13(19): 5344-8.

[41] Xiao L, Tu J, Sun S, Pei Z, Pei Y, Pang Y, et al. A fluorescent probe for hydrazine and its in

vivo applications. Rsc Advances. 2014; 4(79): 41807-11.

[42] [1] Zhang, Shuting, Yu, Haizhu, Meng, Xiangming, et al. A ratiometric two-photon fluorescent probe for hydrazine and its applications. Sensors & Actuators B Chemical. 2015; 220.

[43] Reja SI, Gupta N, Bhalla V, Kaur D, Arora S, Kumar M. A charge transfer based ratiometric fluorescent probe for detection of hydrazine in aqueous medium and living cells. Sensors & Actuators B Chemical. 2016: 222.

[44] Cui L, Ji C, Peng Z, Zhong L, Zhou C, Yan L, et al. Unique tri-output optical probe for specific and ultrasensitive detection of hydrazine. Analytical Chemistry. 2014; 86(9): 4611-7.

[45] Xiao YH, Xi G, Zhao XX, Zhou S, Zhou ZQ, Zhao BX. A Novel Coumarin-Based Fluorescent Probe for the Detection of Hydrazine Both in Aqueous Solution and Vapor State. Journal of fluorescence. 2015; 25(4): 1023-9.

[46] H-Bonding and charging mediated aggregation and emission for fluorescence turn-on detection of hydrazine hydrate. Chemical Communications. 2015; 51(53): 10656-9.

[47] [1] Lipson RH, Shi YJ, Lacey D. An Introduction to Laser Spectroscopy: An Introduction to Laser Spectroscopy, 2002.

[48] Zhou E, Gong S, Feng G. Rapid detection of CO *in vitro* and *in vivo* with a ratiometric probe showing near-infrared turn-on fluorescence, large Stokes shift, and high signal-to-noise ratio. Sensors and Actuators B: Chemical. 2019; 301: 127075-.

[49] Jiang JH, Zhang ZH, Qu J, Wang JY. A lysosomal targeted fluorescent probe based on coumarin for monitoring hydrazine in living cells with high performance. Anal. Methods. 2021; 14(1): 17-21.

[50] Huang J, Zhou Y, Wang W, Zhu J, Li X, Fang M, et al. A fluorescent probe based on

triphenylamine with AIE and ICT characteristics for hydrazine detection. Spectrochim. Acta A Mol. Biomol. Spectrosc. 2023; 286: 122011.

[51] Chen Y, Zhao C, Liu X, Zhang Q, Jiang Y, Shen J. Multi-scene visual hydrazine hydrate detection based on a dibenzothiazole derivative. Analyst. 2023; 148(4): 856-62.

[52] Zeng C, Xu Z, Song C, Qin T, Jia T, Zhao C, et al. Naphthalene-based fluorescent probe for on-site detection of hydrazine in the environment. Journal of hazardous materials. 2023; 445: 130415.

Figure Captions

Scheme. 1 Synthetic procedure for probes **1-3**

Fig. 1. Single crystal structure of probes **1-3** confirmed by single-crystal X-ray diffraction.

Fig. 2. (A) Normalized UV (left) and fluorescence (right) spectra of probes **1-3** in an aqueous solution; (B) The plot of the emission maximum and the relative emission intensity (I/I_0) *versus* the composition of the aqueous mixture of probes **1-3**. Inset: fluorescence photographs of probes **1-3** in the dilute acetonitrile solution and in acetonitrile/water mixtures with 95% water fractions taken under 365 nm UV irradiation.

Fig. 3. Fluorescence (A) and Absorption (B) spectral changes of probe **1** (20 μM) with 80% water content after different testing materials; (C) Fluorescence of probe **1** with metal ions, anions and amino small molecules under 365 nm UV lamp.

Fig. 4. (A) Probe **1** (20 μ M) recognizes the emission intensity of $N_2H_4 \cdot H_2O$ (I_{467}/I_{665}) under interference with other metal ions (A), anions and small amino-containing molecules (B).

Fig. 5. (A) Fluorescence titration spectra of probe **1** (20 μM) with increasing amounts of $N_2H_4 \cdot H_2O$ (0-1.0 equiv.); (B) Linear fitting relationship between the fluorescence intensity of probe **1** and N_2H_4 concentration (0-20 μM); The stability of probe **1** and probe **1** + $N_2H_4 \cdot H_2O$ system *versus* different (C) pH values and (D) reaction time.

Table 1 The determination results for probes **1-3** with hydrazine hydrate.

Fig. 6. The frontier molecular orbitals energy distribution of probe **1** and probe **1**+N_2H_4.

Scheme. 2 Proposed sensing mechanism of probes **1-3** for $N_2H_4 \cdot H_2O$

Fig. 7. Fluorescence images of probe **1** in living HeLa cells. A) HeLa cells were treated with probe **1** (10 μM) for 30 min. B) HeLa cells were firstly treated with probe **1** (10 μM) for 1 h, and then incubated with 10 μM $N_2H_4 \cdot H_2O$ for another 1 h. scale bar = 50

μm.

Fig. 8. Fluorescence images of probe **1** in zebrafish.; (A) zebrafish were loaded with probe **1** (5 μM) for 1 h, (B) zebrafish were pre-loaded with probe **1** (5 μM) for 30 min, and then incubated with 5 μM $N_2H_4 \cdot H_2O$ for another 1 h. scale bar = 200 μm.

Scheme 1.

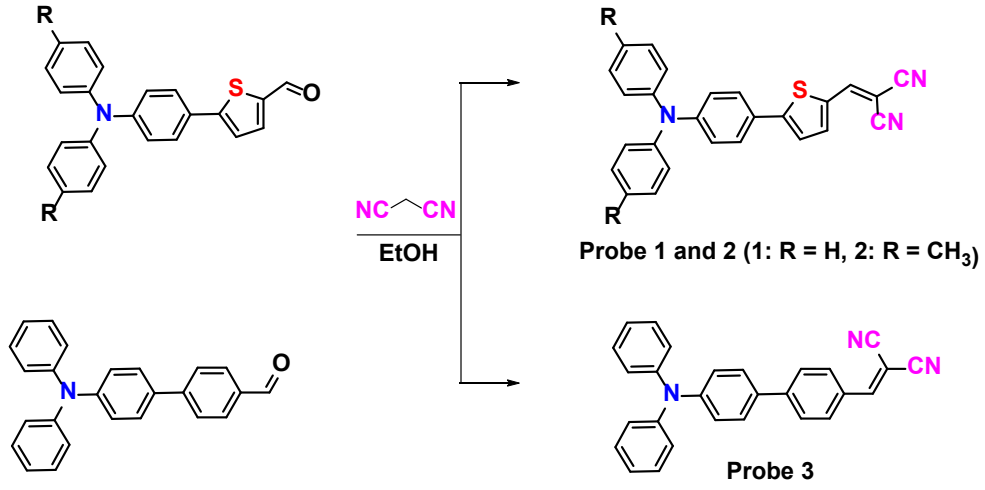

Fig. 1.

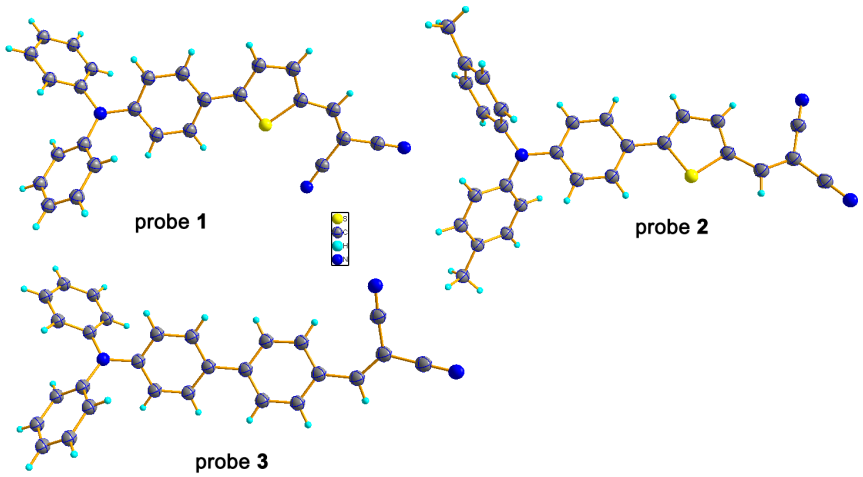
probe 1
probe 2
probe 3

Fig. 2.

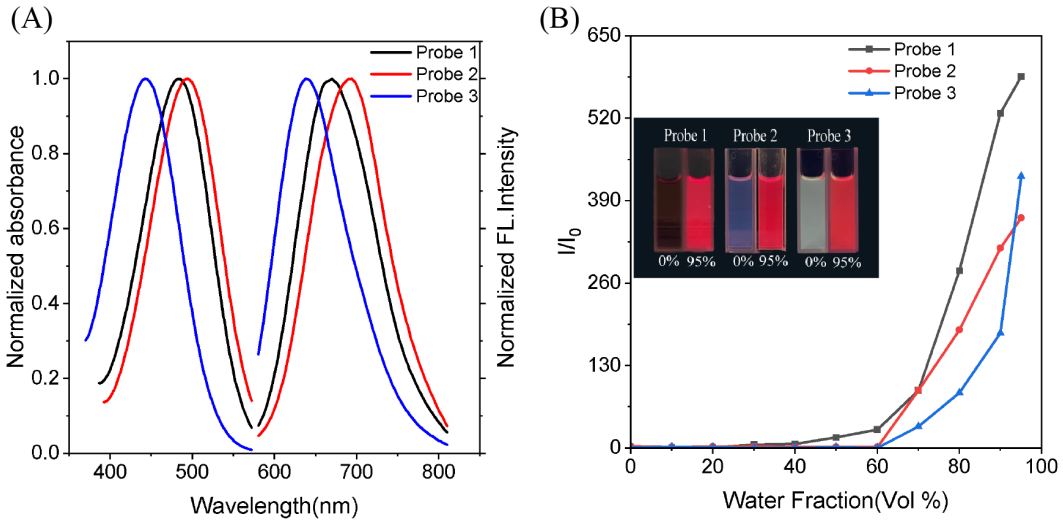
(A)
Probe 1
Probe 2
Probe 3
Normalized absorbance
Normalized FL.Intensity
Wavelength(nm)
(B)
Probe 1
Probe 2
Probe 3
I/I0
Water Fraction(Vol %)
0% 95%
0% 95%
0% 95%

Fig. 3.

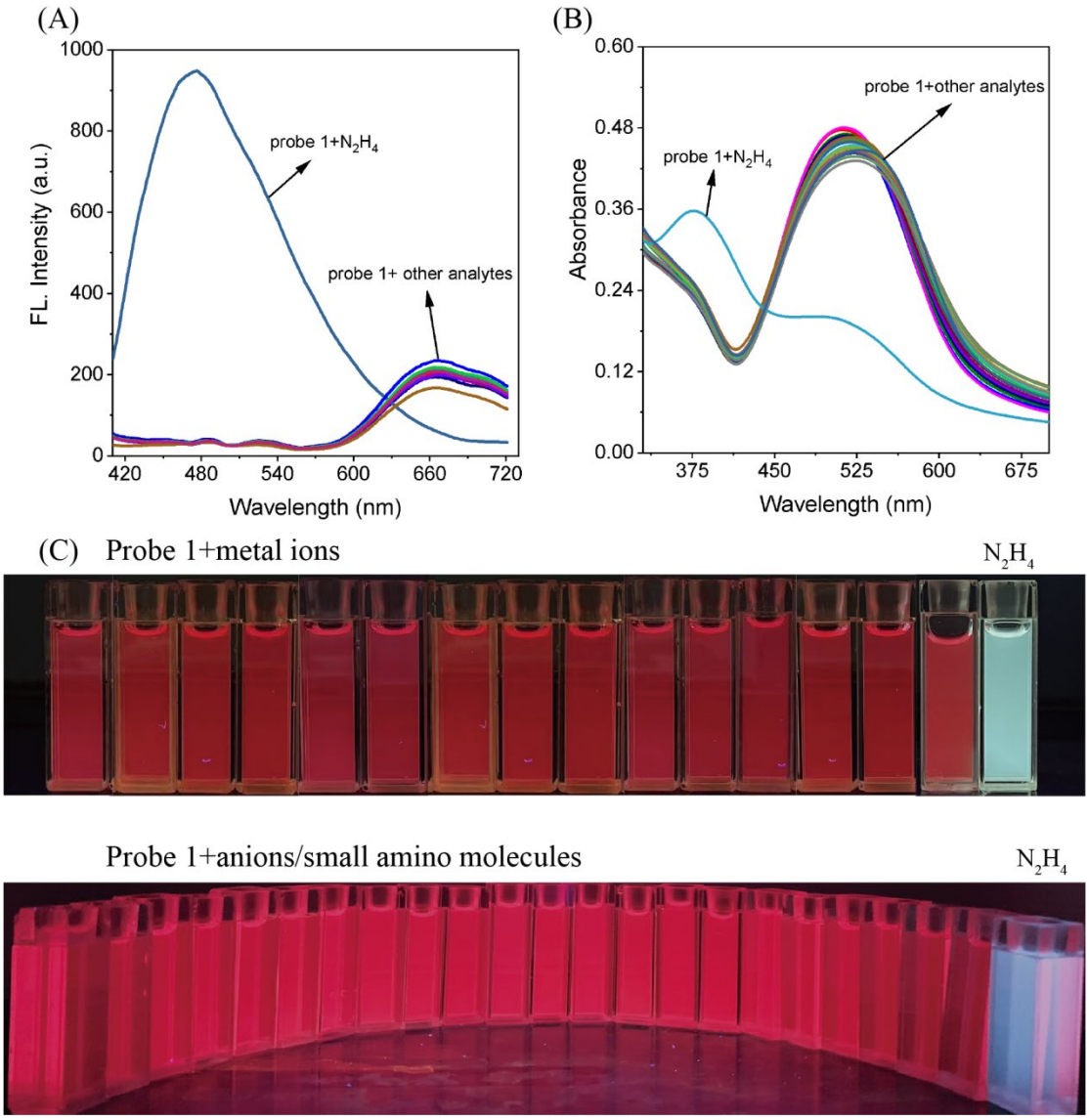
(A)
FL. Intensity (a.u.)
Wavelength (nm)
probe 1+N2H4
probe 1+ other analytes
(B)
Absorbance
Wavelength (nm)
probe 1+N2H4
probe 1+other analytes
(C) Probe 1+metal ions
N2H4
Probe 1+anions/small amino molecules
N2H4

Fig. 4.

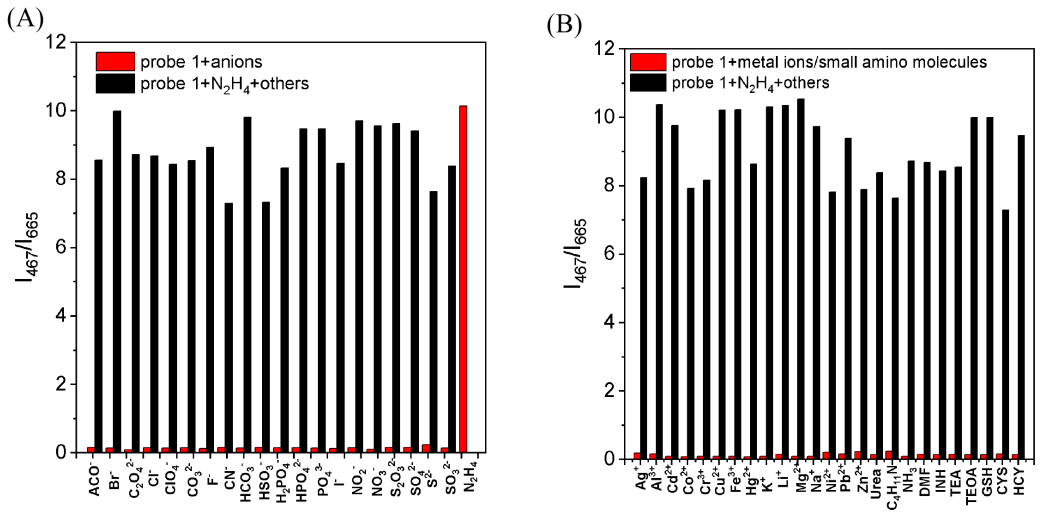
(A)
probe 1+anions
probe 1+N2H4+others
I467/I665
(B)
probe 1+metal ions/small amino molecules
probe 1+N2H4+others
I467/I665

Fig. 5.

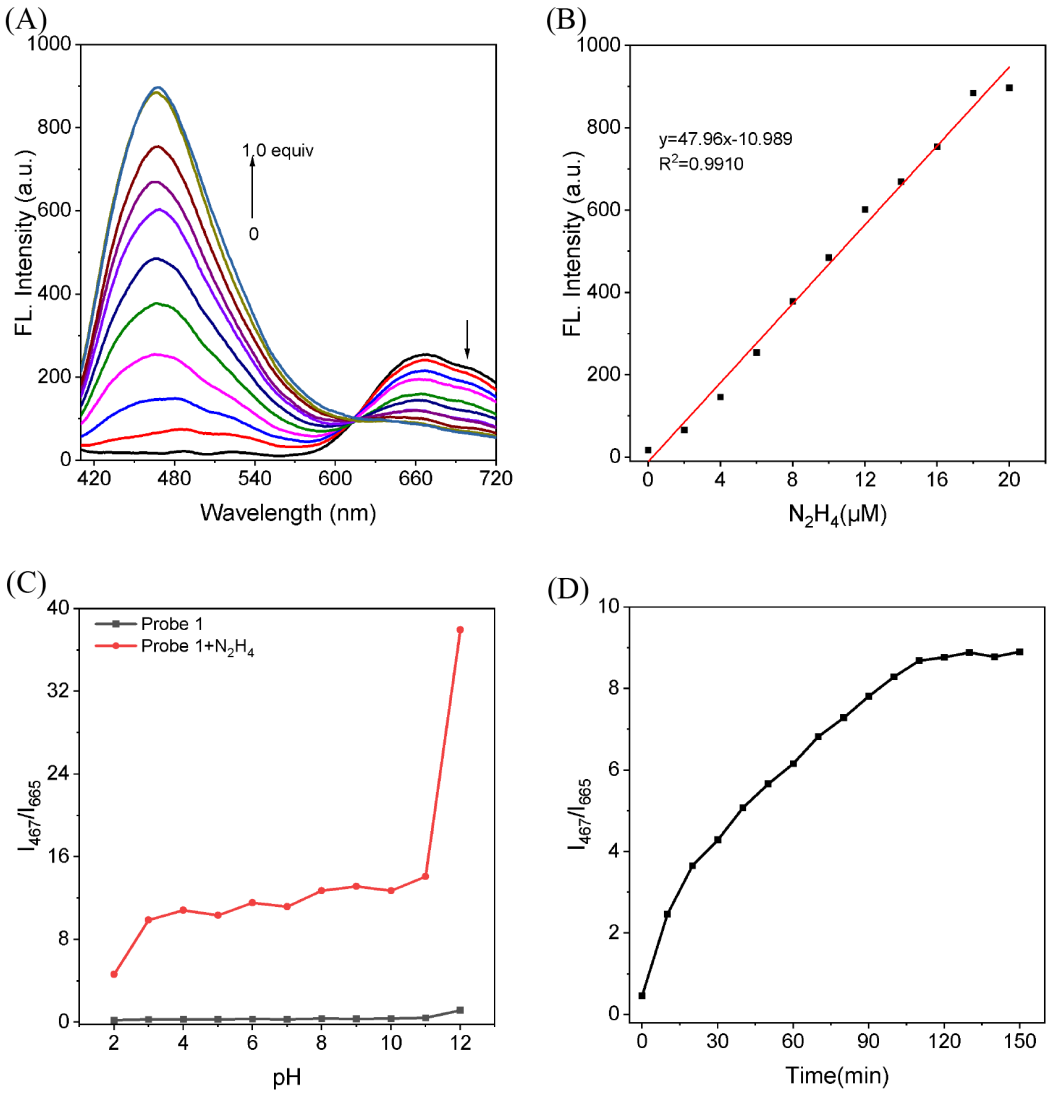

Table 1.

	Probe **1**	Probe **2**	Probe **3**
The detection limit of $N_2H_4 \cdot H_2O$	1.51 μM	0.54 μM	2.61 μM
Suitable pH	3-11	3-11	3-11
Complete reaction time between probe and $N_2H_4 \cdot H_2O$	110 min	110 min	90 min

Fig. 6.

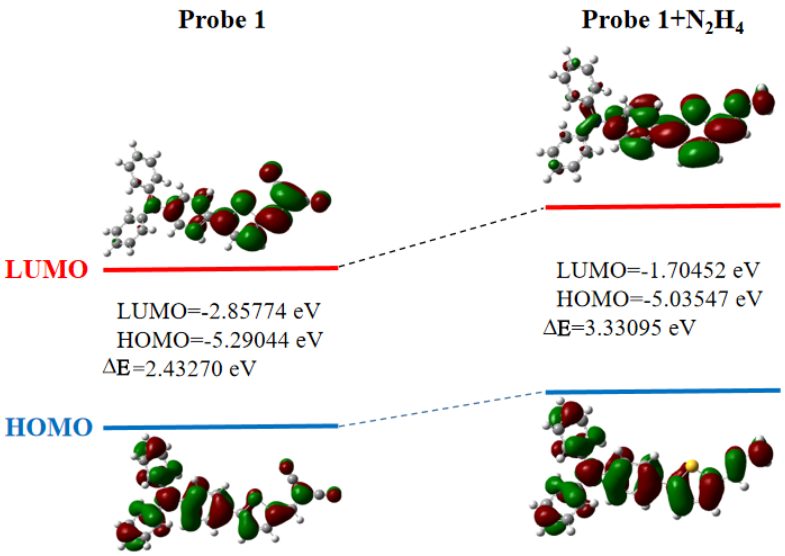

Scheme 2

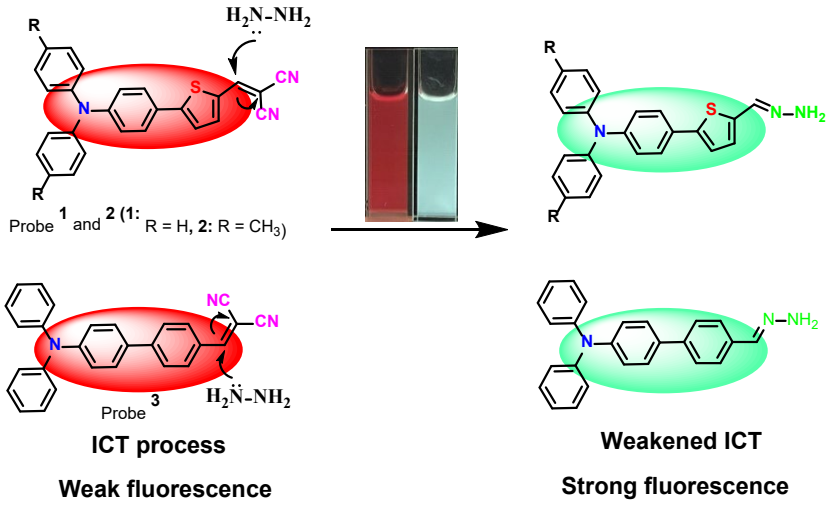

Fig. 7.

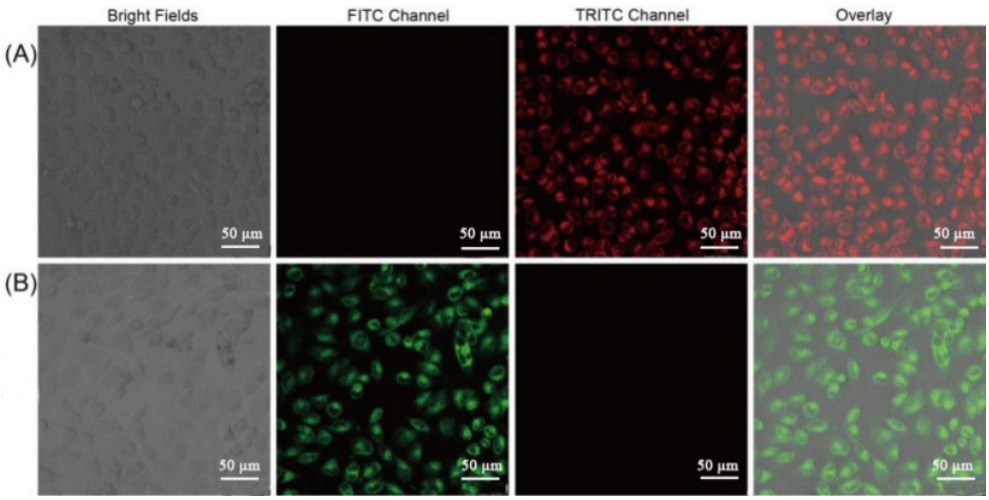
Bright Fields
FITC Channel
TRITC Channel
Overlay
(A)
(B)
50 µm

Fig. 8.

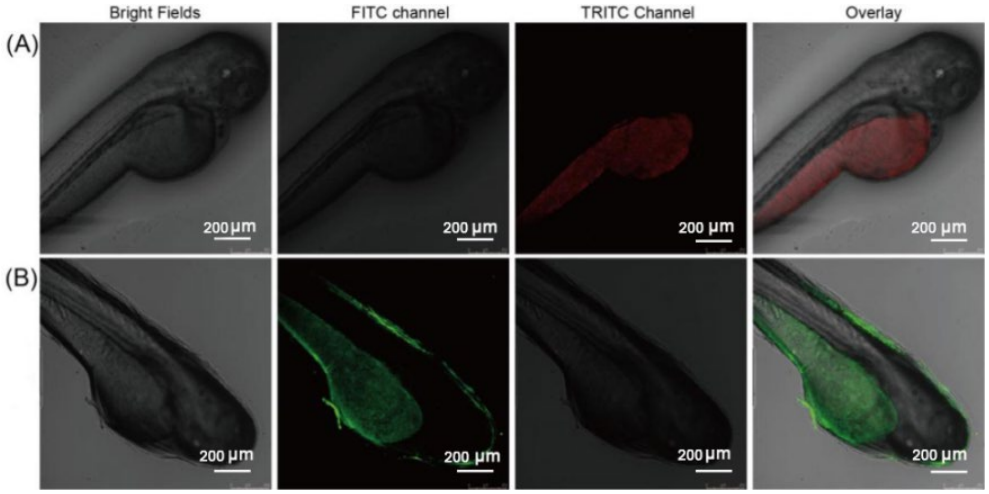
Bright Fields
FITC channel
TRITC Channel
Overlay
(A)
(B)
200 µm